Integral MRAC with Bounded Switching Gain for Autonomous Vehicle Lateral Tracking

Shilp Dixit, Umberto Montanaro, Mehrdad Dianati, Alexandros Mouzakitis, Saber Fallah

***Abstract*—In this paper, an Enhanced Model Reference Adaptive Control (EMRAC) algorithm is used to design a generic lateral tracking controller for an autonomous vehicle. This EMRAC is different from the EMRAC in the literature as it adopts a σ-modification approach to bind the adaptive gains of the switching action of the controller. Moreover, an extended Lyapunov theory for discontinuous systems is used to analytically prove the ultimate boundedness of the proposed closed-loop control system when the adaptive gain of the switching action is bounded with a σ-modification strategy. The control algorithm is applied to a vehicle path tracking problem and its tracking performance is investigated under conditions of (i) external disturbances such as crosswind, (ii) road surface changes, (iii) modelling errors, and (iv) parameter miss-matches in a co-simulation environment based on IPG Carmaker/MATLAB. The simulation studies show that the controller is effective at tracking a given reference path for performing different autonomous highway driving manoeuvres while ensuring the boundedness of all closed-loop signals even when the system is subjected to the conditions mentioned above.**

***Index Terms*—vehicle lateral control; path tracking; autonomous driving; adaptive control.**

I. INTRODUCTION

THe mainstreaming of autonomous vehicles is happening at an increasingly rapid pace in the current decade. The recent push towards autonomous driving has resulted in an ever increased focus of researchers to propose improvements and devise enhancements for the three architectural layers that are typically present in every self-driving platform [1]:

- *Scanning and perception*: responsible for gathering information about the driving conditions in the neighbourhood of the autonomous vehicle
- *Planning*: utilize input from the perception layer to compute a safe and feasible driving trajectory for the vehicle
- *Control*: use the planned trajectory from the planning layer and a reference and compute steering, acceleration, and brake input to make the autonomous vehicle follow the reference trajectory as closely as possible while ensuring the safety and comfort of the occupants

While the top two layers are relative newcomers to the field of automotive engineering, the control layer which mainly involving steering (i.e., lateral/path-tracking control) and throttle/brake control (i.e., longitudinal control) of a vehicle has been a topic of intense research over the past three to four decades [2]. Whereas the initial attempts at lateral controllers were focussed on driver assistance systems (lane-departure warning, lane keeping assistance, etc.), the emphasis in recent years has expanded to a multitude of autonomous driving use-cases ranging from performing complex manoeuvres on public roads (rural, urban, and highways), off-road driving, etc. to motorsport events for autonomous vehicles. There is a vast amount of technical literature available on the different control methods for vehicle lateral control and comprehensive reviews of different controllers are available [3], [4]. These reviews demonstrate that control of lateral dynamics of a vehicle poses a formidable challenge for control engineering due to a combination of reasons such as: (i) significant dependence of lateral dynamics on the longitudinal velocity of a vehicle, (ii) non-linear tire dynamics, (iii) difficulties in estimation of system parameters such as road surface coefficient, vehicle mass distribution, (iv) non-linearities of road/path curvature, etc. The typical control techniques for path-tracking in technical literature are aimed at reducing the lateral position error of the vehicle with respect to the path while ensuring lateral and yaw stability. Researchers have proposed a variety of control techniques to achieve desirable path-tracking performance for an autonomous vehicle [1], [3], [4]. There are control strategies based on geometric constraints such as (i) follow the carrot [3], (ii) Stanley controller [5], and (iii) pure pursuit [3] which have demonstrated their effectiveness in various experimental tests [4], [6]–[8]. Although these control techniques are relatively easy to implement on real-time hardware and provide desired tracking performance around the nominal operational condition, their performance rapidly declines when they operate in different driving conditions [9]. Consequently, other control strategies such as PID, LQR, and sliding mode controllers with feedforward action have been proposed as alternate schemes for lateral control of a vehicle [10], [11]. In these controllers, the feedback controller is designed to reduce the tracking error whereas the feedforward action is developed to counter path curvature. However, it is noted that the LQR controllers have zero gain margin against model uncertainties, sliding-mode controllers suffer from chattering phenomenon, and tuning of PID controllers is not a trivial task making these control strategies difficult to apply over a wide range of path tracking situations [1], [3], [4], [6]. With an increase in available computational resources and development of efficient optimisation solvers, advanced model based control techniques (e.g., Model Predictive Control (MPC)) are also

This work was supported by Jaguar Land Rover and the UK-EPSRC grant EP/N01300X/1 as part of the jointly funded Towards Autonomy: Smart and Connected Control (TASCC) Programme.

S. Dixit, U. Montanaro, and S. Fallah, are with the Department of Mechanical Engineering at University of Surrey, Guildford GU2 7XH, UK (email: {s.dixit,u.montanaro,s.fallah}@surrey.ac.uk).

M. Dianati is with the WMG, International Manufacturing Centre, University of Warwick, Coventry, CV4 7AL, UK (email: m.dianati@warwick.ac.uk).

A. Mouzakitis is with Jaguar Land Rover Limited, Coventry CV3 4LF, UK (email: amouzak1@jaguarlandrover.com).

employed for lateral control of a vehicle [12]–[15]. MPC controllers ranging from standard linear MPC, Linear time-varying (LTV) MPC, and highly complex controllers based on non-linear vehicle and tire models are available in literature [16]–[18]. These advanced control techniques improve tracking performance but their tracking performance is highly sensitive to the accuracy of the system model and hence makes them unsuitable in all driving conditions. The issue of model error is mitigated by nonlinear MPC's but these controllers require large computing resources which makes them impractical for most of the automotive platforms. Recently, active research to augment the abovementioned control techniques with advancements such as neural network, fuzzy logic, etc. to further enhance their applicability and performance has gained great momentum [19]–[23]. However, these techniques rely heavily on readily available training data which is not easily obtainable in the automotive industry. Nevertheless, the difficulties in estimation of system parameters and presence of rapidly changing dynamics due to nonlinearities such as tire dynamics, longitudinal velocity, external disturbances, etc. make vehicle lateral control very challenging problem.

The theoretical framework for adaptive control was formulated over seven decades ago and since then it has been a topic of active research especially for systems that have large dynamic variations and parameter uncertainties [24]. Model Reference Adaptive control (MRAC) is a well-known adaptive control design method and is based on the objective of ensuring that the controlled variables of a plant track a given reference model. This control technique is backed by an established theoretical framework and has proven to be a viable model based control technique especially for systems where real time model parameters are unknown [24]. To improve the tracking of the reference model despite un-modelled system dynamics, system nonlinearities and rapid varying disturbances, in [25] an adaptive integral control action and an adaptive switching control action were added to the standard feedback and feedforward MRAC strategy. The augmented MRAC, also known in the literature as Enhanced MRAC (EMRAC) [26] (see Fig. 1 for a representation of closed-loop control scheme) has shown to be effective at imposing dynamics of the reference model to plants of engineering interest affected by model uncertainties and disturbances such as electronic throttle body [25], common rail systems [27], thermo-hygrometric control [28]. Nevertheless, despite the additional benefits obtained by the auxiliary control action, the concern of unbounded drift of the adaptive control gains leading to degraded tracking performance and/or loss of closed-loop stability has been point of concern for these control schemes. In [29], two different methods namely: (i) parameter-projection and (ii) σ-modification were suggested to prevent unbounded drift of the feedback, feedforward, and integral control gains for systems. The parameter-projection based scheme demonstrated its capability to provide asymptotic zero tracking error and boundedness of adaptive gains even when subjected to transient disturbances. Moreover, when the system is subjected to time-bounded disturbances, the σ-modification scheme guarantees ultimate boundedness of the closed-loop system when subjected to persistent disturbances. However,

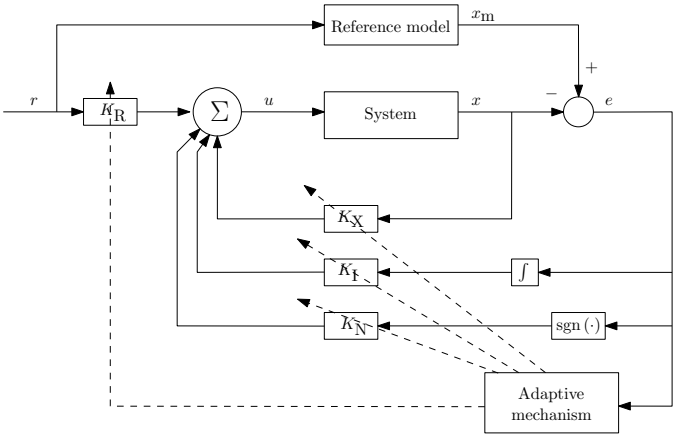

Fig. 1. EMRAC control scheme [26]

only heuristic solutions (saturations) have been suggested to bind the adaptive gain of the switching action [30].

Notwithstanding its ability to handle parameter variations and system nonlinearities and general control flexibility, MRAC schemes for lateral control of a vehicle are marginally studied in literature [31]–[33]. One of the reasons is the concern of unbounded drift of the controller gains leading to instability [34]. In this paper, the σ-modification framework to guarantee bounds on the adaptive control gains discussed above is extended to bind systematically the possible drift in the adaptive switching action gain of the EMRAC. The closed-loop signals system is a piecewise smooth systems and the uniform ultimate boundedness of all the closed loop signals including adaptive gains is proven using the extended Lyapunov theory for non-smooth systems [35]. Moreover, the conditions for the ultimate bound are computed using the above mentioned extended Lyapunov theory [36], [37]. Finally, the adaptive control design is applied to the vehicle path-tracking/lateral control problem. The closed-loop system is implemented on an IPG Carmaker-Simulink co-simulation environment and its behaviour in different driving conditions is investigated. The reference model for the lateral-tracking problem is based on a path-tracking bicycle model from literature [38], [39]. The states of this system capture the dynamics of both, lateral-yaw motion of the vehicle as well as the path deviation errors. A stable reference model is obtained by designing a feedback controller using pole placement for stability along with a feedforward action based on required steady-state cornering behaviour of the vehicle to counter the reference path curvature. This reference model describes the preferred dynamical behaviour of the system for achieving stable cornering while accurately tracking any given reference path curvature that the vehicle might encounter during normal highway driving scenarios.

This paper is structured as follows: Section II introduces the basic symbols and mathematical definitions used in the paper. Section III lays out the mathematical control formulation for the adaptive control scheme together with the analytical proof of the ultimate boundedness of the closed-loop system. The path following system model for the vehicle is discussed in

Section IV. In Section V, the numerical validation of the closed-loop system is carried out in a MATLAB-IPG CarMaker co-simulation environment. Finally, the concluding remarks and future research directions are laid out in Section VI.

II. Mathematical Notations and Definitions

The signum function of a real number x is defined as $\text{sgn}(x) = (d/dx)|x|, \quad x \neq 0$. For a symmetric matrix M and vector x, $||x||_M$ denotes the weighted norm given by $||x||_M = \sqrt{x^T M x}$, $||x||$ denotes the 2-norm of a vector, and $\lambda_{\min}(M)$ and $\lambda_{\max}(M)$ are the minimum and maximum eigenvalue of M, respectively. The matrix $\mathcal{O}_{n,m} \in \mathbb{R}^{n\times m}$ denotes a matrix of zeros, and matrix $\mathcal{I}_n \in \mathbb{R}^{n\times n}$ denotes the identity matrix. For a given vector x, $\text{diag}(x)$ represents a diagonal matrix with x as its diagonal. L_∞ is the set of bounded scalar function. Given a non-smooth time-varying system of the form

$$\dot{\tilde{x}} = \mathfrak{F}(t, \tilde{x}) \tag{1}$$

where $\tilde{x} \in \mathbb{R}^n$ is the state of system and $\mathfrak{F} : \mathbb{R} \times \mathbb{R}^n \to \mathbb{R}^n$ is the discontinuous vector field. Filippov solutions and the concept of differential inclusions allows solutions to be defined at points of discontinuities in the vector field $\mathfrak{F}(t, \tilde{x})$. According to [35], [40] vector function $\tilde{x}(\cdot)$ in $t \in [t_0, t_1]$ is a Filippov solution of the system (1) if: (i) $\tilde{x}(\cdot)$ is an absolutely continuous solution and (ii) for almost all $t \in [t_0, t_1]$

$$\dot{\tilde{x}} \in \mathbf{K}[\mathfrak{F}](t, \tilde{x}) \tag{2}$$

with $\mathbf{K}[\mathfrak{F}](t, \tilde{x})$ being the Filippov set valued map defined as

$$\mathbf{K}[\mathfrak{F}](\tilde{x}) \triangleq \bigcap_{\upsilon>0} \bigcap_{\pi(\mathcal{S})=0} \overline{\text{co}}\{\mathfrak{F}(\mathcal{B}(\tilde{x}, \upsilon) \setminus \mathcal{S})\}, \ \ \tilde{x} \in \mathbb{R}^n \tag{3}$$

where $\bigcap_{\pi(S)=0}$ denotes the intersection of all sets $\mathcal{S}$ of Lebesgue measure zero, $\mathcal{B}(\tilde{x}, \upsilon)$ is the open ball centered at $\tilde{x}$ with radius $\upsilon > 0$, and $\overline{\text{co}}$ denotes the convex closure. Moreover, systems of type (1) with discontinuous right-hand sides also result in non-smooth Lyapunov functions which hinders the use of standard stability theory proofs [35]. Clarke's generalised gradient presented in detail in [41] is a powerful tool that can be used to streamline proofs for non-smooth analysis. For a globally Lipschitz function $V : \mathbb{R}^n \times \mathbb{R} \to \mathbb{R}$, the generalised gradient of V at $(\tilde{x}, t)$ is given by

$$\partial V(\tilde{x}, t) = \overline{\text{co}}\{\lim \nabla V(\tilde{x}, t) | (\tilde{x}_i, t_i) \to (\tilde{x}, t), (\tilde{x}_i, t_i) \notin \Xi_V\} \tag{4}$$

where Ξ_V is the set of measure zero where the gradient of V is not defined [35]. It is noteworthy that Lipschitz means Lipschitz in $(\tilde{x}, t)$ and discontinuities in t are not allowed. Furthermore, if $V(\tilde{x}, t)$ has no explicit dependence on t, the last component of ∂V can be dropped as it is zero. The generalised directional derivative of V is defined in [35] as

$$V^\circ(\tilde{x}; \gamma) = \lim_{\tilde{y}\to\tilde{x},} \sup_{t\downarrow 0} \frac{V(\tilde{y} + t\gamma) - V(\tilde{y})}{t} \tag{5}$$

and if V is Lipschitz near $\tilde{x}$, then

$$V^\circ(\tilde{x}; \gamma) = \max\{\langle \xi, \gamma \rangle \ | \ \xi \in \partial V(\tilde{x})\} \tag{6}$$

Thus, by using the definitions in (5), (6), a function V is called a regular function if the following two conditions are fulfilled [35]

- $\forall \gamma$, the one-sided directinoal derivative of $V'(\tilde{x}; \gamma)$ exists,
- $\forall \gamma$, $V'(\tilde{x}; \gamma) = V^\circ(\tilde{x}; \gamma)$.

According to Theorem 2.2 in [35] if $\tilde{x}(\cdot)$ is a solution to (1) and $V(\tilde{x}, t)$ is a regular function, then $(d/dt)V(\tilde{x}, t)$ exists almost everywhere and it can be computed as

$$\frac{d}{dt} V(\tilde{x}, t) \in^{\text{a.e}} \dot{\tilde{V}}(\tilde{x}, t) \tag{7}$$

where

$$\dot{\tilde{V}} = \bigcap_{\xi \in \partial V(\tilde{x}, t)} \xi^{\text{T}} \begin{pmatrix} \mathbf{K}[\mathfrak{F}](t, \tilde{x}) \\ 1 \end{pmatrix} \tag{8}$$

The solutions of the system in the form (1) are said to be uniformly ultimately bounded [42] if; there exists a time interval T (dependent on $\tilde{x}(t_0)$) and a $\mathcal{KL}-$class function $\Psi : \mathbb{R}^+ \times \mathbb{R}^+ \to \mathbb{R}^+$ such that

$$||\tilde{x}(t)|| \leq \Psi(||\tilde{x}(t_0)||, t - t_0) \ \ \forall t \in [t_0, t_0 + T] \tag{9a}$$

and:

$$||\tilde{x}|| \leq \epsilon \ \ \forall t \in [t_0, t_0 + T] \text{ and } \epsilon > 0 \tag{9b}$$

The aforementioned definitions and theorems have been recently used in [43] to formulate the conditions that guarantee the ultimate boundedness of the discontinuous system described in (1) and the main theorem is reported below.

Theorem II.1. Assume that for any initial conditions, the differential inclusion (2) for system (1) is well-posed in the sense of Filippov solutions, and there exists a positive globally Lipschitz continuous function $V : \mathbb{R}^n \to \mathbb{R}$, two positive functions $W_1, W_2 \in \mathcal{K}_\infty$, and $W_3 \in \mathcal{K}$ such that

$$W_1(\tilde{x}) \leq V(\tilde{x}, t) \leq W_2(\tilde{x}) \tag{10a}$$

$\exists \mu > 0$, such that

$$\dot{\tilde{V}}(\tilde{x}, t) \leq -W_3(\tilde{x}), \text{ when } ||\tilde{x}|| \geq \mu \tag{10b}$$

with $\dot{\tilde{V}}(\tilde{x}, t)$ being the generalised gradient of V, then the non-smooth system in (1) is globally uniformly ultimately bounded. It is noteworthy that Theorem II.1 is a special case of Theorem 3.1 in [43] by assuming (i) zero the time delays, (ii) the solution of the differential inclusion (2) exists for any initial condition, and (iii) $V(\tilde{x}, t)$ is defined over the entire $\mathbb{R}^n$.

III. Control Formulation

Consider a plant modelled in the form

$$\dot{x} = Ax + B_1 u + B_2 r + B_1 d \tag{11}$$

where $x \in \mathbb{R}^n$, $u \in \mathbb{R}$, $r \in \mathbb{R}$, and $d \in \mathbb{R}$ are the state, actuated input, un-actuated input, and the disturbance of the system, respectively. The disturbance acting on the plant is assumed to belond to L_∞, thus there exists Δ_∞ such that $|d| < \Delta_\infty$. The structure of the system matrices $A \in \mathbb{R}^{n\times n}$, $B_1 \in \mathbb{R}^n$, and $B_2 \in \mathbb{R}^n$ are assumed to be known and constructed from the nominal parameters of the given system. The control objective

is to steer the dynamics of the system (11) towards those of an asymptotically stable LTI reference system of the form

$$\dot{x}_{\mathrm{m}} = A_{\mathrm{m}} x_{\mathrm{m}} + B_{\mathrm{m}} r \tag{12}$$

where $x_{\mathrm{m}} \in \mathbb{R}^n$ is the reference model state, and $A_{\mathrm{m}} \in \mathbb{R}^{n\times n}$, $B_{\mathrm{m}} \in \mathbb{R}^n$ are the reference model system matrices with A_{m} being Hurwitz. By assuming that there exist two constant matrices K_{X}^* and K_{R}^* such that the following matching conditions are satisfied

$$A_{\mathrm{m}} = A + B_1 K_{\mathrm{X}}^* \tag{13a}$$
$$B_{\mathrm{m}} = B_1 K_{\mathrm{R}}^* + B_2 \tag{13b}$$

The aforementioned model reference control problem is solved by the EMRAC control action

$$u(t) = K_{\mathrm{X}}(t)x(t) + K_{\mathrm{R}}(t)r(t) + K_{\mathrm{I}}(t)e_{\mathrm{I}}(t) + K_{\mathrm{N}}(t)\mathrm{sgn}(y_e(t)) \tag{14}$$

where the state tracking error is defined as

$$e = x_{\mathrm{m}} - x \tag{15}$$

and e_{I} is the integral of the state tracking error e. The output error y_e is defined as

$$y_e = C_e e, \text{ with } C_e = B_1^{\mathrm{T}} P \text{ and } P A_{\mathrm{m}} + A_{\mathrm{m}}^{\mathrm{T}} P = -Q \tag{16}$$

with Q being a positive definite matrix and the solution P of the Lyapunov equation in (16) exists as A_{m} is Hurwitz. The adaptive control gains K_{X}, K_{R}, and K_{I} are computed as in [29]. Differing from the solutions available in literature, in this work K_{N} is bounded by including the σ-modification strategy into the adaptive law of K_{N}, thus avoiding the use of heuristic solutions (saturations of the gain). Hence, K_{N} is adapted as

$$K_{\mathrm{N}} = \phi_{\mathrm{N}} \text{ and } \dot{\phi}_{\mathrm{N}} = \alpha_{\mathrm{N}}|y_e| + f_{\mathrm{N}} \tag{17}$$

where α_{N} is a positive constant and f_{N} is the σ-modification term defined as:

$$f_{\mathrm{N}} = -\rho_{\mathrm{N}} \cdot \sigma_{\phi_{\mathrm{N}}}(||\phi_{\mathrm{N}}||) \cdot \phi_{\mathrm{N}} \tag{18a}$$

$$\sigma_{\phi_{\mathrm{N}}}(||\phi_{\mathrm{N}}||) = \begin{cases} 0 & \text{if } ||\phi_{\mathrm{N}}|| \le \hat{\mathcal{M}}_{\phi_{\mathrm{N}}} \\ \eta_{\phi_{\mathrm{N}}}\left(\dfrac{||\phi_{\mathrm{N}}||}{\hat{\mathcal{M}}_{\phi_{\mathrm{N}}}} - 1\right) & \text{if } \hat{\mathcal{M}}_{\phi_{\mathrm{N}}} < ||\phi_{\mathrm{N}}|| \le 2\hat{\mathcal{M}}_{\phi_{\mathrm{N}}} \\ \eta_{\phi_{\mathrm{N}}} & \text{if } ||\phi_{\mathrm{N}}|| > 2\hat{\mathcal{M}}_{\phi_{\mathrm{N}}} \end{cases} \tag{18b}$$

where $\hat{\mathcal{M}}_{\phi_{\mathrm{N}}}$, $\eta_{\phi_{\mathrm{N}}}$, and ρ_{N} are positive constants and

$$\eta_{\phi_{\mathrm{N}}} > \frac{3}{4} \cdot \alpha_{\mathrm{N}}^{-1} \cdot \rho_{\mathrm{N}} \cdot \lambda_{\min}(Q) \tag{19}$$

Theorem III.1. Consider system (11) with $r, d \in L_\infty$ and the reference model (12). Let the adaptive control action be given by (14), with the adaptive gain for the discontinuous action computed as in (17). Then all resultant closed-loop signals are bounded and the state of the closed-loop system is globally uniformly ultimately bounded.

Before providing the proof for Theorem III.1, the following lemma is given.

Lemma III.2. Similar to Lemma 2 from [29], an additional set of guarantees given below can be derived:

$$\phi_{\mathrm{N}e}\alpha_{\mathrm{N}}^{-1} f_{\mathrm{N}} \ge 0, \ \forall \phi_{\mathrm{N}} \in \mathbb{R} \tag{20a}$$
$$\phi_{\mathrm{N}e}\alpha_{\mathrm{N}}^{-1} f_{\mathrm{N}} > 0, \ \forall \phi_{\mathrm{N}} : ||\phi_{\mathrm{N}}|| \ge \hat{\mathcal{M}}_{\phi_{\mathrm{N}}} \tag{20b}$$
$$\phi_{\mathrm{N}e}\alpha_{\mathrm{N}}^{-1} f_{\mathrm{N}} > \frac{\eta_{\phi_{\mathrm{N}}}}{2}\phi_{\mathrm{N}e}^{\mathrm{T}}\alpha_{\mathrm{N}}^{-1}\rho_{\mathrm{N}}\phi_{\mathrm{N}e}, \ \forall \phi_{\mathrm{N}} : ||\phi_{\mathrm{N}}|| > 2\hat{\mathcal{M}}_{\phi_{\mathrm{N}}} \tag{20c}$$

Proof of Lemma III.2:

The proof of the lemma above follows the same steps as those in the proof of Lemma 2 in [29] and is excluded here for brevity.

Proof of Theorem III.1:

The proof of the theorem above is based on two steps, i.e., (i) recast the closed-loop system as a Filippov system and (ii) prove the existence of a positive definite function V that satisfies Theorem II.1.

Closed-loop dynamics: By considering the plant in (11), the reference model in (12), the control action in (14), and the matching condition in (13) and performing some algebraic manipulations, the equations of the closed-loop dynamics can be expressed as

$$\dot{e} = A_{\mathrm{m}} e + B_1[\phi_e^{\mathrm{T}} w - y_e w^{\mathrm{T}}\Gamma_\beta w + \phi_{\mathrm{N}e}\mathrm{sgn}(y_e) - d] \tag{21a}$$
$$\dot{\phi}_e = -y_e \Gamma_\alpha w - f \tag{21b}$$
$$\dot{\phi}_{\mathrm{N}e} = -\alpha_{\mathrm{N}}|y_e| + f_{\mathrm{N}} \tag{21c}$$
$$\text{with } w^{\mathrm{T}} = [x^{\mathrm{T}}, r, e_{\mathrm{I}}^{\mathrm{T}}], \ w \in \mathbb{R}^{2n+1}$$

and ϕ_e being the vector collecting the mis-matches between the plant parameters and the integral parts of the adaptive gains K_{X}, K_{R}, and K_{I} (see [29] for its mathematical definition), Γ_α and $\Gamma_\beta \in \mathbb{R}^{(2n+1)\times(2n+1)}$ are the positive matrices representing the adaptive weights for the integral part and the proportional part of K_{X}, K_{R}, and K_{I} repectively, and f is the σ-modification limiting the evolution of their integral part (see [29] for its mathematical definition). It is noteworthy that due to the discontinuities arising from the switching action of the controller, the vector field in (21) expressed as $\mathfrak{F} : \mathbb{R} \times \mathbb{R}^{3n+2} \to \mathbb{R}^{3n+2}$ is a piecewise system. Thus, using the mathematical formulation in (1) and (2), the closed-loop system in (21) can be described by the differential inclusion

$$\dot{\tilde{x}} \in \mathbf{K}[\mathfrak{F}](\tilde{x}) \tag{22}$$

where $\mathbf{K}[\mathfrak{F}](\tilde{x})$ represents the Filippov set-valued map of the piecewise system and $\tilde{x}^{\mathrm{T}} = [e^{\mathrm{T}}, \phi_e^{\mathrm{T}}, \phi_{\mathrm{N}e}]$.

Existence of Candidate Lyapunov Function V: The candidate Lyapunov function is

$$V(\tilde{x}) = \tilde{x}^{\mathrm{T}}\tilde{P}\tilde{x} \tag{23}$$

where $\tilde{P} = \mathrm{diag}(P, \Gamma_\alpha^{-1}, \alpha_{\mathrm{N}}^{-1})$, with P being the solution of the Lyapunov equation in (16). It is noteworthy that (23) can be bounded as [29], [42]

$$W_1(\tilde{x}) \le V(\tilde{x}) \le W_2(\tilde{x}) \tag{24}$$

where $W_1(\tilde{x}) = \lambda_{\min}(\tilde{P})||\tilde{x}||^2$ and $W_2(\tilde{x}) = \lambda_{\max}(\tilde{P})||\tilde{x}||^2$. As V is a smooth function and by extension a regular function [35], [42], [43], $(d/dt)V(\tilde{x})$ exists and can be computed as in (7). Therefore, by using (22) the derivative of (23) along the closed-loop trajectories (21) can be expressed as

$$\frac{d}{dt}V(\tilde{x}) \in^{\text{a.e}} \dot{\tilde{V}}(\tilde{x}) = \bigcap_{\xi \in \partial V(\tilde{x})} \xi^{\mathrm{T}} \mathbf{K}[\boldsymbol{\mathcal{f}}](\tilde{x}) \tag{25}$$

According to [35], since $V(\tilde{x})$ is a smooth function

$$\dot{\tilde{V}}(\tilde{x}) = \nabla V^T \cdot \mathbf{K}[\boldsymbol{\mathcal{f}}](\tilde{x}) \tag{26}$$

$$\dot{\tilde{V}}(\tilde{x}) \subset 2 \begin{bmatrix} e \\ \phi_e \\ \phi_{\mathrm{N}e} \end{bmatrix}^{\mathrm{T}} \tilde{P} \cdot \mathbf{K}[\boldsymbol{\mathcal{f}}](\tilde{x}) \tag{27}$$

The differential inclusion $\mathbf{K}[\boldsymbol{\mathcal{f}}](\tilde{x})$ in (22) can be expanded as

$$\mathbf{K}[\boldsymbol{\mathcal{f}}] = \mathbf{K} \begin{bmatrix} A_{\mathrm{m}}e + B_1[\phi_e^{\mathrm{T}}w - y_e w^{\mathrm{T}}\Gamma_\beta w + \phi_{\mathrm{N}e}\text{sgn}(y_e) - d] \\ -y_e\Gamma_\alpha w - f \\ -\alpha_{\mathrm{N}}|y_e| + f_{\mathrm{N}} \end{bmatrix} \tag{28a}$$

$$= \begin{bmatrix} A_{\mathrm{m}}e + B_1[\phi_e^{\mathrm{T}}w - y_e w^{\mathrm{T}}\Gamma_\beta w + \phi_{\mathrm{N}e}\mathbf{K}[\text{sgn}(y_e)] - d] \\ -y_e\Gamma_\alpha w - f \\ -\alpha_{\mathrm{N}}|y_e| + f_{\mathrm{N}} \end{bmatrix} \tag{28b}$$

After some algebraic manipulations, using the Lyapunov equation in (16), and the differential inclusion in (28) the right hand side of (27) is

$$\begin{aligned} \dot{\tilde{V}}(\tilde{x}) = &- e^{\mathrm{T}}Qe - 2y_e^2 w^{\mathrm{T}}\Gamma_\beta w + 2y_e\phi_{\mathrm{N}e}\mathbf{K}[\text{sgn}(y_e)] - \\ &2y_e d - 2\phi_e^{\mathrm{T}}\Gamma_\alpha^{-1}f - 2\phi_{\mathrm{N}e}|y_e| - 2\phi_{\mathrm{N}e}\alpha_{\mathrm{N}}^{-1}f_{\mathrm{N}} \end{aligned} \tag{29}$$

Note that $\mathbf{K}[\text{sgn}(y_e)]$ is a set-valued map that is computed as

$$\mathbf{K}[\text{sgn}(y_e)] = \begin{cases} -1 & , \ y_e < 0 \\ [-1, 1] & , \ y_e = 0 \\ 1 & , \ y_e > 0 \end{cases} \tag{30}$$

Thus, after further simplification (29) can be upper bounded as

$$\dot{\tilde{V}}(\tilde{x}) \leq -e^{\mathrm{T}}Qe - 2y_e d - 2\phi_e^{\mathrm{T}}\Gamma_\alpha^{-1}f - 2\phi_{\mathrm{N}e}\alpha_{\mathrm{N}}^{-1}f_{\mathrm{N}} \tag{31}$$

It is noted that, to obtain (31), the term $2y_e\phi_{\mathrm{N}e}\mathbf{K}[\text{sgn}(y_e)]$ is cancelled by $-2\phi_{\mathrm{N}e}|y_e|$ when $y_e \neq 0$ and both terms are zero when $y_e = 0$. The first three terms on the right hand side of (31) have been considered in [29] and the equation above can be further manipulated as in the proof of Theorem 2 in [29] by using the same steps. Thus, $\dot{\tilde{V}}$ can be further upper-bounded as:

$$\begin{aligned} \dot{\tilde{V}}(\tilde{x}) \leq &-\frac{3}{4}\lambda_{\min}(Q)||e||^2 + 4\frac{||B_1 P||^2}{\lambda_{\min}(Q)}|d|^2 - \\ &2\phi_e^{\mathrm{T}}\Gamma_\alpha^{-1}f - 2\phi_{\mathrm{N}e}\alpha_{\mathrm{N}}^{-1}f_{\mathrm{N}} \end{aligned} \tag{32}$$

By defining

$$\tilde{\Gamma}_\alpha^{-1} = \text{diag}(\Gamma_\alpha^{-1}, \alpha_{\mathrm{N}}^{-1}) \tag{33a}$$

$$\tilde{f} = \begin{bmatrix} f \\ f_{\mathrm{N}} \end{bmatrix} \tag{33b}$$

$$\tilde{\phi}_e = \begin{bmatrix} \phi_e \\ \phi_{\mathrm{N}e} \end{bmatrix} \tag{33c}$$

the expression in (32) becomes the following.

$$\dot{\tilde{V}}(\tilde{x}) \leq -\frac{3}{4}\lambda_{\min}(Q)||e||^2 + 4\frac{||B_1 P||^2}{\lambda_{\min}(Q)}|d|^2 - 2\tilde{\phi}_e^{\mathrm{T}}\tilde{\Gamma}_\alpha^{-1}\tilde{f} \tag{34}$$

It is noted that $\dot{\tilde{V}}$ is then upper-bounded as in the proof of Theorem 2 in [29], thus it can be further manipulated by using the same steps in [29], thus

$$\dot{\tilde{V}}(\tilde{x}) \leq -W_3(\tilde{x}), \text{ where } ||\tilde{x}|| \geq \mu \tag{35}$$

where $W_3(\tilde{x})$ is defined as

$$W_3(\tilde{x}) = \theta\alpha||\tilde{x}||^2, \text{ where } ||\tilde{x}|| \geq \mu; \ \alpha, \theta \in (0, 1) \tag{36a}$$

$$\mu = \sqrt{\frac{\mu_2}{\mu_1(1-\theta)}} \tag{36b}$$

$$\mu_1 = \frac{3}{4}\lambda_{\min}(Q) \tag{36c}$$

$$\mu_2 = 3\frac{||B_1 P||^2}{\mu_1}\Delta_\infty^2 + \mu_1(2\hat{\mathcal{M}}_\phi + ||\phi^*|| + 2\hat{\mathcal{M}}_{\phi_{\mathrm{N}}})^2 \tag{36d}$$

and $\hat{\mathcal{M}}_\phi$ and ϕ^* are the threshold and the ideal control gains define defined in [29], respectively. Consequently, by considering (24) and (35), the closed-loop dynamics (21) satisfy all the conditions in Theorem II.1. Thus, the closed-loop system is ultimately bounded with the ultimate bound given below.

$$W_1^{-1}(W_2(\mu)) = \sqrt{\frac{\lambda_{\max}(\tilde{P})}{\lambda_{\min}(\tilde{P})}}\mu \tag{37}$$

IV. Path Tracking Model

The primary objective of a path tracking controller is to accurately follow the reference path under a wide range of operating conditions. Path tracking for autonomous vehicles is a particularly challenging task as the dynamics of a vehicle change significantly with changes in longitudinal velocity, road surface, external disturbances such as wind, challenging manoeuvres etc. The initial generation of path tracking controllers were based on geometric controllers (e.g., Stanley, follow the carrot, etc.) and were shown to provide suitable performance under nominal conditions both in simulation and real world experiments. However, their performance suffers when the system deviates far from nominal conditions and thus prompted researchers to develop more advanced control algorithms (e.g., sliding mode control, robust control, adaptive control, MPC, etc.) that were suitable for the complex nature of the problem. In this section, the path-following system model is presented and the application of the control law in (14) to an autonomous vehicle's lateral control problem is discussed. In order to apply the control law in (14), the relevant vehicle

and error states of the system need to be expressed in the format given in (11). To capture the relevant lateral and yaw dynamics of the autonomous vehicle, the single-track dynamic bicycle model of the vehicle is utilized, (see Fig. 2). The vehicle's lateral velocity v_y and yaw rate r_z are used to get a representation of the vehicle's dynamics. Additional states that are augmented to this model are, (i) the lateral position error defined as the lateral distance error from the Centre of Gravity (C.G.) of the vehicle from the desired path η_e, measured perpendicularly to the vehicle's orientation and (ii) the heading angle error ψ_e, defined as the difference between the orientation of the vehicle and the desired yaw angle. The equations that describe the evolution of the four states have been described in [38], [44] and have also been used by researchers to develop their lateral-yaw tracking controller for autonomous vehicles [38].

$$\begin{bmatrix} \dot{v}_y \\ \dot{r}_z \\ \dot{\eta}_e \\ \dot{\psi}_e \end{bmatrix} = \begin{bmatrix} \frac{C_\mathrm{f}+C_\mathrm{r}}{Mv_x} & \frac{l_\mathrm{f}C_\mathrm{f}+l_\mathrm{r}C_\mathrm{r}}{Mv_x} - Mv_x & 0 & 0 \\ \frac{l_\mathrm{f}C_\mathrm{f}-l_\mathrm{r}C_\mathrm{r}}{MI_z} & \frac{l_\mathrm{f}^2C_\mathrm{f}+l_\mathrm{r}^2C_\mathrm{r}}{v_xI_z} & 0 & 0 \\ -1 & 0 & 0 & v_x \\ 0 & -1 & 0 & u \end{bmatrix} \begin{bmatrix} v_y \\ r_z \\ \eta_e \\ \psi_e \end{bmatrix} + \begin{bmatrix} -\frac{C_\mathrm{f}}{M} \\ -\frac{l_\mathrm{f}C_\mathrm{f}}{I_z} \\ 0 \\ 0 \end{bmatrix} \delta_\mathrm{f} + \begin{bmatrix} 0 \\ 0 \\ 0 \\ v_x \end{bmatrix} \kappa \tag{38}$$

where $x^\mathrm{T} = [v_y, r_z, \eta_e, \psi_e]$ are the states of the system, the front wheel steering angle $u = \delta_\mathrm{f}$ is the actuated input, and the desired path curvature $r = \kappa$ is the unactuated input to the system. Moreover, by defining the system matrices as

$$A = \begin{bmatrix} \frac{C_\mathrm{f}+C_\mathrm{r}}{Mv_x} & \frac{l_\mathrm{f}C_\mathrm{f}+l_\mathrm{r}C_\mathrm{r}}{Mv_x} - Mv_x & 0 & 0 \\ \frac{l_\mathrm{f}C_\mathrm{f}-l_\mathrm{r}C_\mathrm{r}}{MI_z} & \frac{l_\mathrm{f}^2C_\mathrm{f}+l_\mathrm{r}^2C_\mathrm{r}}{v_xI_z} & 0 & 0 \\ -1 & 0 & 0 & v_x \\ 0 & -1 & 0 & u \end{bmatrix} \tag{39a}$$

$$B_1^\mathrm{T} = \begin{bmatrix} -\frac{C_\mathrm{f}}{M} & -\frac{l_\mathrm{f}C_\mathrm{f}}{I_z} & 0 & 0 \end{bmatrix} \tag{39b}$$

$$B_2^\mathrm{T} = \begin{bmatrix} 0 & 0 & 0 & v_x \end{bmatrix} \tag{39c}$$

the system in (38) can be expressed in the compact form given below.

$$\dot{x} = Ax + B_1u + B_2\kappa \tag{40}$$

For normal road-going vehicle, the system matrix A in (40) has two poles in the negative half plane (stable lateral dynamics of understeered vehicle) and two poles on the origin (from the error states), resulting in an unstable system. It is noteworthy that the matrices A and B_1 are dependent on the vehicle parameters (mass, weight distribution, moment of inertia, tire cornering stiffness, etc.) and generally nominal values of these parameters are used to create the system model. However, the entries of the matrices of the plant are not precisely known because of plant parameter uncertainties

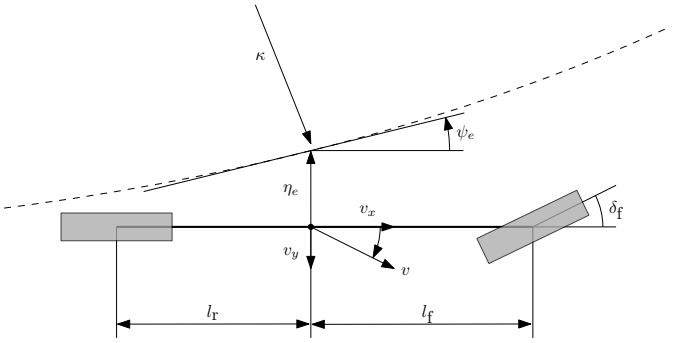

Fig. 2. Overview of path-tracking model. Note: Reference path (black-dashed)

and variation of the longitudinal speed, thus opening the need of adaptive solutions. In general, a combination of feedback and feedforward control law is designed to obtain accurate path tracking of the autonomous vehicle. The feedback control is used to stabilise the system and achieve desired path-tracking performance. However, if the unactuated control input i.e., κ is very large (representing tight highway turns/curves), a feedback control can lead to large lateral position errors and thus, an appropriate feedforward controller is utilized to counter the road curvature input and theoretically achieve zero steady-state lateral position error. A typical control law implementation involves designing a control law of the form [38]:

$$u = K_\mathrm{FB}(v_x)x + K_\mathrm{FF}(v_x, \kappa)\kappa \tag{41}$$

The application of the control law from (41) for a given set of nominal vehicle parameters and a given longitudinal speed results in the following closed-loop dynamics of the system in (40)

$$\dot{x} = (A + B_1K_\mathrm{FB}^*)x + (B_1K_\mathrm{FF}^* + B_2)\kappa \tag{42}$$

where K_FB^* and K_FF^* represent the nominal feedback and feedforward controller based on default vehicle parameters. Successful implementation of the resultant closed-loop control scheme law in experimental tests have demonstrated their ability at tracking the curvature of tight highway corners under medium to high-speed driving $(70 - 120\,\mathrm{km\,h^{-1}})$ scenarios. However, due to the controlled nature of the testing environments, it is yet to be seen how they cope with variations such as rapidly changing road friction, wind gusts, vehicle parameter variations, etc. which are possible scenarios an autonomous vehicle will face during its operation beyond controlled test environments. It is noteworthy, that from an occupant acceptance point of view, it will be advantageous to have a system that can provide uniformity in its behaviour despite changes in system parameters or external perturbation i.e., the vehicle should perform the same manoeuvre in a uniform manner under different internal and/or external perturbations. To this effect, the system dynamics are modelled as

$$\dot{x} = Ax + B_1u + B_2\kappa + B_1d \tag{43}$$

where $d \in \mathbb{R}$ is a bounded disturbance acting upon the system and contains the deviation between a nominal system model

and the actual system due to modeling miss-match, parameter variation, external disturbances, degradation, etc. A control law that steers the dynamics of the system in (43) to the reference system in (42) where the system matrices in (12) are selected as $A_{\rm m} = A + B_1 K^*_{\rm FB}$ and $B_{\rm m} = B_1 K^*_{\rm FF} + B_2$, while fulfilling three requirements of: (i) ensuring lateral stability of system, (ii) providing accurate path tracking, and (iii) assuring the uniformity of system dynamics over entire operating range can be a viable option for real world usage and user acceptance. Subsequently, an MRAC based control formulation presented in Section III can be a viable framework to achieve the three requirements mentioned above. Moreover, ensuring boundedness of all the adaptive gains using the σ-modification technique means that the inputs and states will not need to be artificially saturated like previous implementations of MRAC in autonomous vehicles [31]–[33]. Thus, the control law in (14)-(18) is designed for a system model in (43). The resultant controller is then implemented in a MATLAB-IPG CarMaker co-simulation (closed-loop) structure with the CarMaker environment providing the high-fidelity plant dynamics. In the following section, this implementation is explained in further detail and the efficacy of the proposed control law for steering control of an autonomous vehicle is shown using a number of simulation studies.

V. Numerical Validation

As mentioned in the section above, the ability of the control law in (14)-(18) to impose the desired vehicle path is done in a MATLAB-IPG CarMaker co-simulation environment. The simplified system model in (38) is created using the nominal vehicle parameters obtained from the IPG vehicle model. A reference model of the form (42) is created in two steps namely: (i) the feedback controller is designed using the pole placement method by introducing two stable poles for the error states while keeping the stable poles of v_y, r_z intact, and (ii) computing a reference feedforward based on the equations from [44]. The MRAC is then designed using the techniques discussed in Section III and the resultant control law is connected in closed-loop with the high-fidelity vehicle and system model from IPG CarMaker. This results in a closed-loop structure as illustrated in Fig. 1. It is noteworthy that the task of longitudinal control is assigned to the default Adaptive Cruise Controller (ACC) provided by the IPG CarMaker platform. The closed-loop simulation is performed for different manoeuvres to mimic typical driving conditions that an autonomous vehicle might encounter in a highway environment. These simulations are designed to numerically evaluate the performance of the proposed controller when it encounters combination of typical issues such as: (i) modelling errors, (ii) disturbances, (iii) rapidly changing disturbances, etc. The design parameters used for the simulation platform are provided in Table I.

A. Manoeuvre I: Navigating a hypothetical highway section

In this section, the controller's ability to track a reference vehicle model over a large highway road segment while ensuring boundedness of control inputs is demonstrated. The hypothetical highway segment consists of straight driving sections interspersed with four corners of different radii, see Fig. 3 (top). The tightest of these corners corresponds to a curve of radius which is approximately equal to the tightest corner allowed on highways [38]. During the simulation the proposed tracking controller will control the steering of the vehicle to track the road curvature whereas as mentioned above, the standard ACC from IPG will be used to maintain the desired vehicle velocity (i.e., $107\,\mathrm{km\,h^{-1}}$). On performing the simulation, it was observed that the ACC is unable to keep very tight control over the longitudinal velocity of the vehicle and as a result the longitudinal velocity of the vehicle is not maintained constant during the entirety of the manoeuvre, Fig. 3 (bottom). Furthermore, the manoeuvre is also simulated without locking the evolution of the adaptive gain of the switching control action (referred henceforth as ctrl0). Thus, this simulation test can be used to gain insight on three important aspects namely: (i) behaviour of closed-loop system, (ii) evolution of adaptive control gains, and (iii) ability of controller to counter variations in parameters of system/plant. The evolution of the adaptive gains $K_{\rm X}$, $K_{\rm R}$, and $K_{\rm I}$ when the adaptive switching action is bounded using σ-modification over the entire simulation can be observed in Fig. 4 which confirm their bounded evolution. Fig. 5 depicts the evolution of $||\phi_{\rm N}||$ and the evolution of the magnitude of the integral part of the gains $K_{\rm X}$, $K_{\rm R}$, and $K_{\rm I}$ denoted as $||\phi||$. As shown in the top plot of Fig. 5, the evolution of $||\phi||$ does not remarkably change when the σ-modification strategy for $||\phi_{\rm N}||$ is activated. However, the evolution of $||\phi_{\rm N}||$ in bottom plot of Fig. 5 clearly exhibits one of the main contributions of this paper. When there is no locking strategy the control gain for the switching action is unbounded and keeps on increasing. On the other hand, preventing the unbounded evolution of $||\phi_{\rm N}||$ using a σ-modification strategy is also illustrated. The closed-loop dynamics of the system and the evolution of the system states are presented in Fig. 6. According to the plots, the closed-loop performance obtained with and without bounding the $||\phi_{\rm N}||$ are very similar if not identical. Both, the states representing vehicle lateral-yaw dynamics (i.e., v_y and r_z) and the error states (i.e., η_e and ψ_e) closely match the reference closed-loop dynamics during the entire manoeuvre.

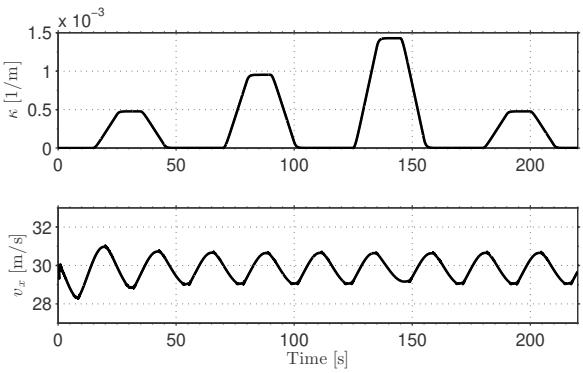

Fig. 3. Reference road curvature and longitudinal velocity for hypothetical highway driving scenario (Manoeuvre I)

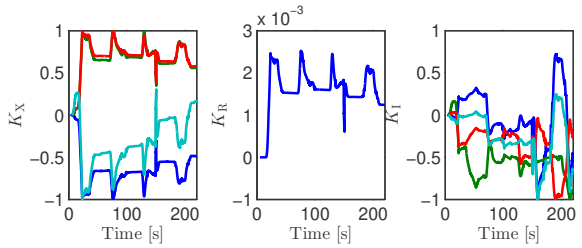

Fig. 4. Evolution of K_{X}, K_{R}, and K_{I} for hypothetical highway driving scenario (Manoeuvre I)

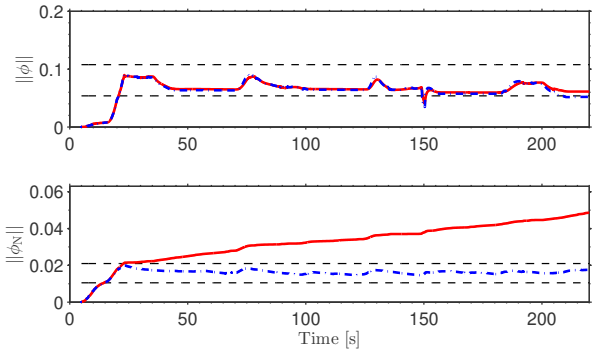

Fig. 5. Evolution of $||\phi||$ and $||\phi_{\mathrm{N}}||$ for hypothetical highway driving scenario (Manoeuvre I). Note: Unbounded switching action (Red), gain of the switching action bounded by σ-modification (Blue-dashed)

However, close inspection (of especially v_y and r_z) towards the end of the simulation shows that the behaviour of the two controllers seems to be diverging. Further insight on this behaviour can be gained by observing the evolution of the state error plotted in Fig. 7. The absolute magnitude of the error helps in confirming that both controllers achieve accurate tracking of the reference model. However, while negotiating the final curve of the manoeuvre which is identical to the first curve, the performance of the controller with unbounded evolution of $||\phi_{\mathrm{N}}||$ visibly deteriorates. The plot insets show that the error for the first two states (and by extension the states v_y and r_z) for ctrl0 have oscillatory behaviour akin to chattering whose amplitude and frequency appears to be increasing with time. This oscillatory behaviour in the lateral-yaw dynamics of the system has a negative impact not only on the stability of the system but also on the comfort of the occupants. On the contrary, when evolution of $||\phi_{\mathrm{N}}||$ is bounded controller exhibits no such degradation and there is no introduction of chattering like behaviour in the state or error dynamics. Since, both controllers have very similar evolution of $||\phi||$, the consistency in the performance of the proposed controller (Figs. 6 and 7) and its advantages can be traced to the successful implementation of a locking strategy for $||\phi_{\mathrm{N}}||$ (see both plots in Fig. 5). The applied control action with and without bounding the gain $||\phi_{\mathrm{N}}||$ is shown in Fig. 8. While the general control action applied by both the controllers is very similar, the larger spikes that get introduced in the control action for ctrl0 after $50\,\mathrm{s}$ are easily observable. As seen from the plots above, this more aggressive control action does not bring any tangible benefits to the closed-loop performance and after approximately $150\,\mathrm{s}$ this aggressive control action damages the closed-loop performance giving rise to high-frequency oscillations. Furthermore, the plot inset in Fig. 8 illustrates that while the proposed controller does not suffer from any chattering like problem, the same cannot be said for ctrl0. Interestingly, the deviation in the control action of the two controllers can be traced back to the time when the $||\phi_{\mathrm{N}}||$ uncontrollably increased beyond the bounds around $50\,\mathrm{s}$ as clearly seen in Fig. 5. Thus, successfully utilising the σ-modification strategy to lock the gain of the switching action of the control law allows the resultant closed-loop system to maintain its performance even with un-modelled non-linearities of the plant.

B. Manoeuvre II: Driving in crosswind

A common source of disturbance while traveling on highways is crosswinds. Crosswinds that are blowing across the vehicle's path are especially dangerous if not actively countered as they tend to veer a vehicle of its intended path/lane and can lead to extremely dangerous consequences (e.g., roll over, collisions with other vehicles, leaving built road, etc.). Moreover, the location and magnitude of crosswinds is difficult to measure/estimate and thus successfully rejecting

TABLE I
DESIGN PARAMETERS

Symbol	Value	Units	Symbol	Value	Units
System Parameters			Adaptive Controller Parameters		
l_{f}	1.446	m	ρ_{X}	$10^{-3}\mathcal{I}_4$	-
l_{r}	1.477	m	ρ_{R}	10^{-3}	-
M	2412.503	kg	ρ_{I}	$10^{-3}\mathcal{I}_4$	-
I_z	4715.977	$\mathrm{kg\,m^2}$	ρ_{N}	8×10^{-4}	-
C_{f}	3.4781×10^5	$\mathrm{N\,rad^{-1}}$	α_{X}	$[42,42,420,210]^{\mathrm{T}}$	-
C_{r}	3.4781×10^5	$\mathrm{N\,rad^{-1}}$	α_{R}	500	-
$v_{x,\mathrm{nom}}$	29.8611	$\mathrm{m\,s^{-1}}$	α_{I}	$[4.2,4.2,42,21]^{\mathrm{T}}$	-
Reference Controller Parameters			α_{N}	0.35	-
K_{X}^*	$[-0.0615,-0.157,0.03735,4.4651]$	-	β_{X}	$\alpha_{\mathrm{X}}/20$	-
K_{R}^*	$[4.8145]$	-	β_{R}	$\alpha_{\mathrm{R}}/20$	-
Adaptive Controller Parameters			β_{I}	$\alpha_{\mathrm{I}}/20$	-
$\mathcal{M}$	0.0049	-	η_ϕ	2	-
$\hat{\mathcal{M}}_{\phi_{\mathrm{N}}}$	0.0105	-	$\eta_{\phi_{\mathrm{N}}}$	30	-

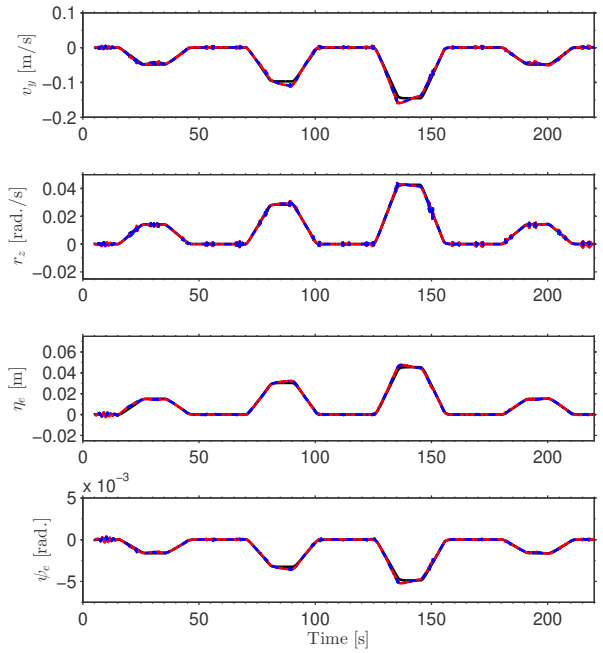

Fig. 6. Dynamics of system for hypothetical highway driving scenario (Manoeuvre I). Note: Unbounded switching action (Red), gain of the switching action bounded by σ-modification (Blue dashed), reference model (solid black)

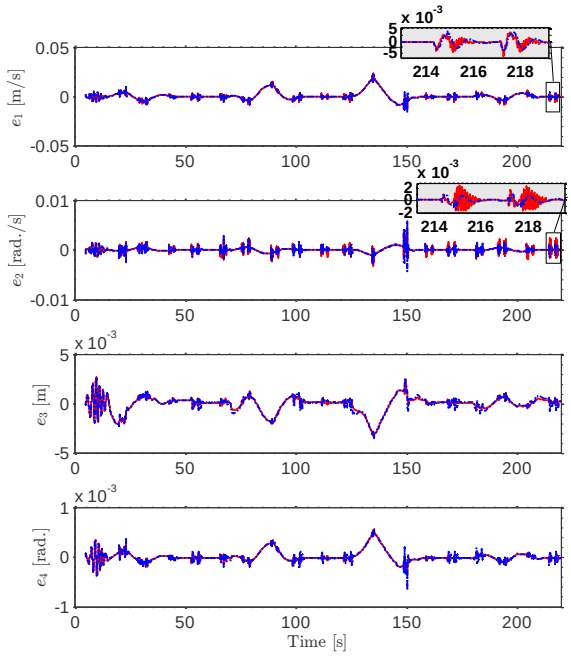

Fig. 7. Evolution of state errors for hypothetical highway driving scenario (Manoeuvre I). Note: Unbounded switching action (Red), gain of the switching action bounded by σ-modification (Blue-dashed), reference model (Solid black)

their effects forms an important challenge for any trajectory tracking controller. In this section, the controller's capability to reject sudden large gust of crosswind is assessed. The scenario is as explained: the autonomous vehicle is driving on a straight road while maintaining the desired velocity (i.e., $107\,\mathrm{km\,h^{-1}}$) and at about $3.45\,\mathrm{s}$ the vehicle encounters crosswind blowing at $110\,\mathrm{km\,h^{-1}}$ perpendicular to the path of the vehicle for a duration of $3.55\,\mathrm{s}$. The scenario explained above is simulated twice. Once with no active steering control and the second time with the proposed controller. The main results of the simulation test are as follows.

The system dynamics of the vehicle are presented in Fig. 9 where both, the uncontrolled vehicle and the vehicle controlled with the proposed controller are shown. It is noteworthy that the dynamics of the reference model are not plotted here for the clarity readability of plots but the reader is reminded that since the vehicle is assumed to be traveling on a straight piece of road, the reference states are constant (i.e., $x_{\mathrm{m}}^{\mathrm{T}} = [0, 0, 0, 0]$). Moreover, the duration of the simulation when the vehicle is subjected to the crosswind is marked with the yellow rectangle. The third and the fourth plot in Fig. 9 show that the uncontrolled vehicle get blown off the road as soon as it encounters the wind gust thus re-emphasising the need for closed-loop control techniques in autonomous vehicles to actively counter such environmental disturbances. On the other hand, on encountering the wind gust, the vehicle with active control recovers quickly to regulate the lateral velocity v_y, and yaw-rate r_z of the vehicle. This limits the increase in the lateral error η_e and heading angle error ψ_e which means that the vehicle follows the reference states (and by extension reference path/lane) as accurately as possible. A zoomed in plot of the evolution of the lateral error state is shown in the third plot of Fig. 9. The plot demonstrates that while there is a peak deviation of approximately due to crosswind, the controller is able to prevent its further rise. Furthermore, the magnitude of the error is very small compared to a typical lane width (i.e., $3.5\,\mathrm{m}$) which means that no safety violations occur and the entire vehicle safely remains within its lane limits.

In general, the switching action of the controller is added to continuous control action to reject the effect of such large and sudden external disturbances. The evolution of the switching

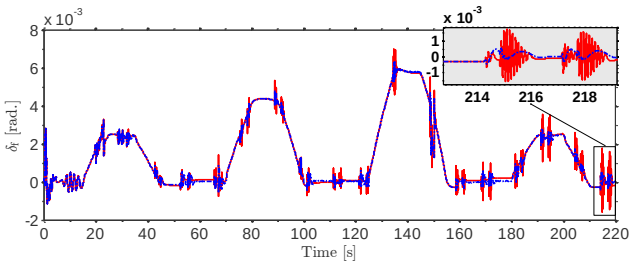

Fig. 8. Net control input for hypothetical highway driving scenario (Manoeuvre I). Note: Unbounded switching action (Red), gain of the switching action bounded by σ-modification (Blue-dashed)

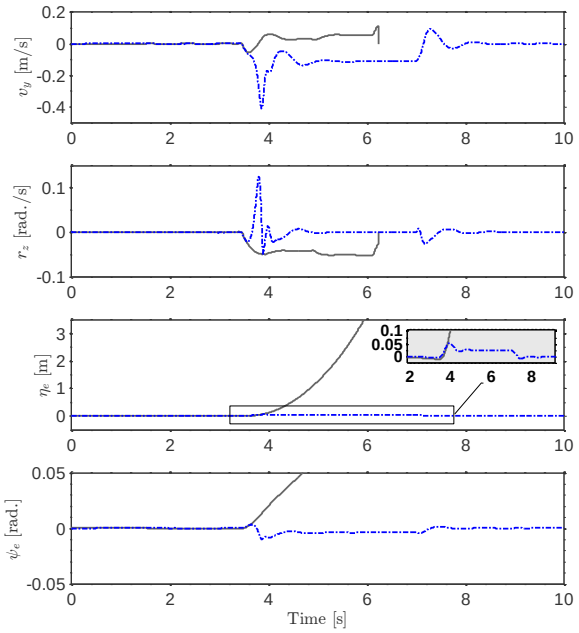

Fig. 9. Dynamics of system for driving in crosswinds (Manoeuvre II). Note: Uncontrolled (Grey), Switching action bounded by σ-modification (Blue-dashed)

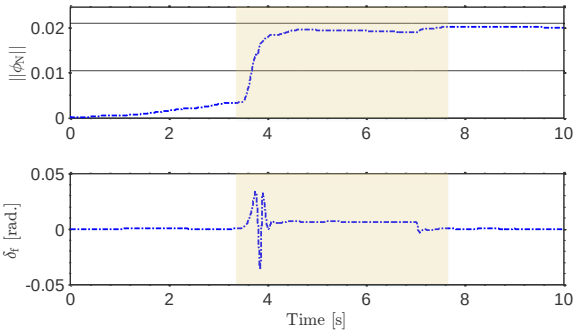

Fig. 10. Evolution of $||\phi_{\mathrm{N}}||$ and control input for driving in crosswinds (Manoeuvre II)

action gain is shown in top plot of Fig. 10. The plot shows that the switching gain increases rapidly on the onset of the disturbance but the σ-modification technique helps in limiting its unbounded rise for the remaining manoeuvre. The control action that is applied is illustrated in the bottom plot of Fig. 10. The advantage of having a switching action within the control law assists the initial phase of large actuation as soon as the wind gust is encountered. Furthermore, the locking strategy ensures that the switching action does not become dominant.

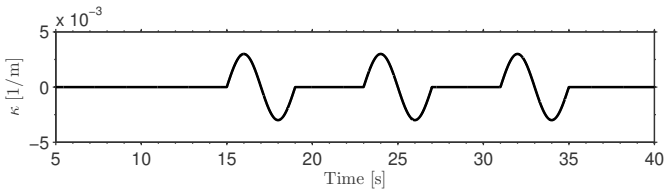

Fig. 11. Reference road curvature for lane changes in low friction (Manoeuvre III)

C. Manoeuvre III: Lane change in low friction conditions with additional passengers

In this section, the closed-loop performance of the system when there is a large mismatch between the reference model and the actual plant is evaluated. This scenario is created by: (i) changing the friction coefficient of road from its nominal value ($\mu_{\mathrm{road,ref}} = 0.8$) to a hypothetical road covered with snow/ice ($\mu_{\mathrm{road}} = 0.4$) and (ii) two additional passengers weighing 75 kg are added on the rear-seat of the vehicle. This has the combined effect of changing the plant parameters (e.g., $M, I_z, C_{\mathrm{f}}, C_{\mathrm{r}}, l_{\mathrm{f}}, l_{\mathrm{r}}$) such that the dynamics of the plant are different from the nominal model used for control design. This closed-loop system is then simulated on the given icy road segment and the vehicle is subjected to three lane-change manoeuvres (see Fig. 11) and the ability of the trajectory tracking controller to counter this large model miss-match while performing these manoeuvres is investigated. It is noteworthy that such deviations of the actual system from nominal plant dynamics are very common for autonomous vehicles as they are operated in a diverse range of conditions all across the parameter range. Thus, it is important for a tracking controller to be truly roadworthy, it needs to ensure uniform closed-loop dynamics for the vehicle across such diverse conditions.

The closed-loop dynamics of the system is presented in Fig. 12 and the corresponding error dynamics are shown in Fig. 13. The closed-loop dynamics of the system under the same manoeuvre but with the plant also under nominal conditions is also plotted to gain better insight on the controller's behaviour. The first two plots in Fig. 12 demonstrate that the initial vehicle response when subjected to the first lane change differs in amplitude from the nominal vehicle (and the reference vehicle). The direct consequence of this is greater deviation from the reference path as observed from the error states in the bottom two plots of Fig. 12. However, safety of the manoeuvre is never compromised since the controller adapts to the model miss-match and pushes the system dynamics towards the reference (and nominal) system dynamics. By the time the vehicle is subjected to the third lane-change manoeuvre, the closed-loop system appears to have adapted and the trajectories of all the states almost converge with the reference (and nominal) model. Some of these insights can also be obtained by observing the error plots in Fig. 13. These plots illustrate how the magnitude of error gets smaller with each subsequent lane change manoeuvre thus showing that the controller adapts to the changes quickly and helps in ensuring that the system maintains its fundamental closed-

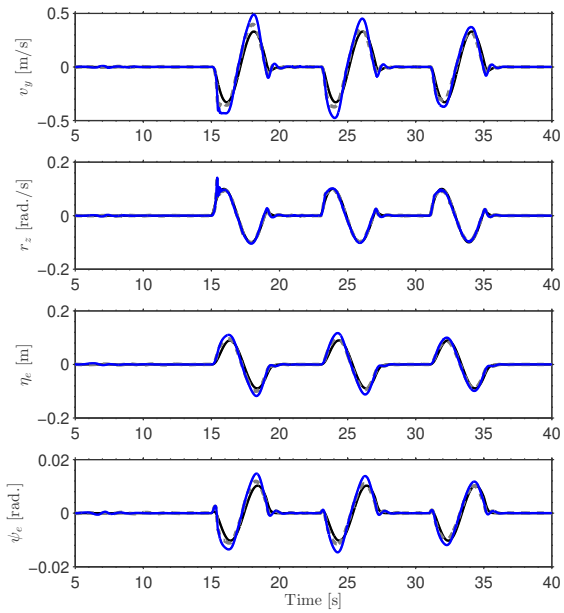

Fig. 12. Dynamics of system for lane changes in low friction (Manoeuvre III). Note: Nominal conditions (Grey-dashed), low-friction and extra passengers (Blue)

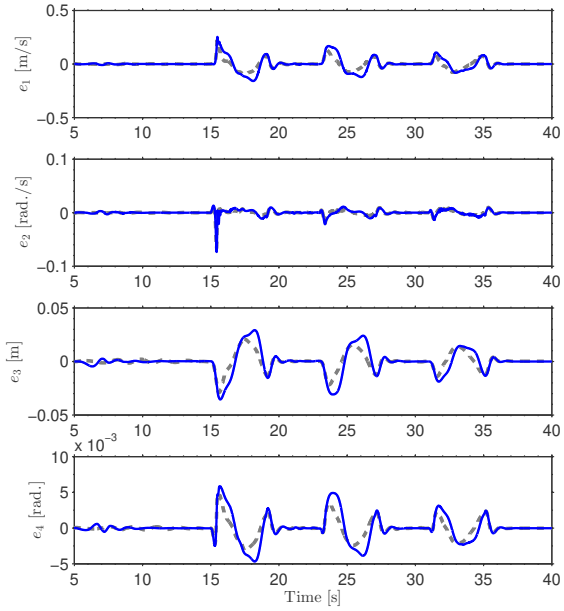

Fig. 13. Evolution of state errors for lane changes in low friction (Manoeuvre III). Note: Nominal conditions (Grey-dashed), low-friction and extra passengers (Blue)

loop behaviour even when subjected to large variations in plant parameters.

The evolution of the switching action is presented in the top plot of Fig. 14. The differences in the initial evolution of the gain up to 15 s are clearly visible. However, in the locking region of the controller, the evolution of $||\phi_N||$ is very similar

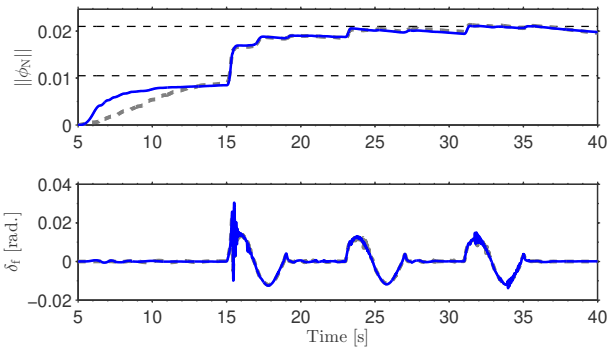

Fig. 14. Evolution of $||\phi_N||$ and control input for lane changes in low friction (Manoeuvre III). Note: Nominal conditions (Grey-dashed), low-friction and extra passengers (Blue)

and the σ-modification strategy is able to successfully ensure that the locking policy works effectively.The net control action applied by the controller is shown in the bottom plot of Fig. 14. There is an initial transient in the control action (i.e., at 15 s) which is largely due to the activation of the control action but the subsequent control action for the remaining portion of the simulation is smooth without any high-frequency content which highlights the benefits of preventing unbounded increase in the gain of switching control action.

VI. Conclusion

Lateral tracking of an autonomous vehicle for following a given reference path is a challenging task due to inherent aspects of the system such as external disturbances, system nonlinearities, rapidly changing dynamics, etc. arising due to tire dynamics, wind gusts, road surface changes, modelling miss-matches, etc. In this paper, a generic lateral tracking controller has been designed using an Enhanced Model Reference Adaptive Control (EMRAC) strategy due to its ability to maintain closed-loop performance even for systems that are affected by the phenomenon mentioned above. Furthermore, a systematic technique of binding the gain of the switching control action of the EMRAC controller using σ-modification strategy has been presented. The ultimate boundedness of the resulting closed-loop system is proven using an extended Lyapunov theory for discontinuous systems. The effectiveness of the EMRAC control framework with bounded adaptive gains is numerically evaluated by designing a lateral controller for a vehicle and investigating the closed-loop performance under different scenarios in an IPG CarMaker-Simulink co-simulation environment. The evaluation performed over three representative examples showed that the proposed controller can achieve effective closed-loop performance even when the system is subjected to large external disturbances, modelling errors, etc. while ensuring bounded evolution of adaptive control gain of the switching control action thus providing numeric validation of the proposed method to confine its dynamics. As part of future work, the lateral tracking controller investigated in the paper will be tested under a larger

set of manoeuvres and driving conditions leading to further experimental validation.

ACKNOWLEDGMENT

This work was supported by Jaguar Land Rover and the UK-EPSRC grant EP/N01300X/1 as part of the jointly funded Towards Autonomy: Smart and Connected Control (TASCC) Programme.

REFERENCES

[1] S. Dixit, S. Fallah, U. Montanaro, M. Dianati, A. Stevens, F. Mccullough, and A. Mouzakitis, "Trajectory planning and tracking for autonomous overtaking: State-of-the-art and future prospects," *Annual Reviews in Control*, vol. 45, pp. 76–86, 2018.

[2] S. E. Shladover, "PATH at 20—History and major milestones," *IEEE Transactions on Intelligent Transportation Systems*, vol. 8, no. 4, pp. 584–592, 2007.

[3] N. Hafizah, A. Hairi, K. Hudha, and Z. Abdul, "Modelling and Control Strategies in Path Tracking Control for Autonomous Ground Vehicles : A Review of State of the Art and Challenges," *Journal of Intelligent & Robotic Systems*, vol. 86, no. 2, pp. 225–254, 2016.

[4] A. Sorniotti, P. Barber, and S. D. Pinto, "Path Tracking for Automated Driving: A Tutorial on Control System Formulations and Ongoing Research," in *Automated Driving: Safer and More Efficient Future Driving*. Springer, 2017, pp. 71–140.

[5] S. Thrun, M. Montemerlo, H. Dahlkamp, D. Stavens, A. Aron, J. Diebel, P. Fong, J. Gale, M. Halpenny, and G. Hoffmann, "Stanley: The robot that won the DARPA Grand Challenge," *Journal of Field Robotics*, vol. 23, no. 9, pp. 661–692, 2015.

[6] J. M. Snider, "Automatic Steering Methods for Autonomous Automobile Path Tracking," *Robotics Institute, Pittsburgh, PA, Tech. Rep. CMU-RITR-09-08*, 2009.

[7] V. Cerone, M. Milanese, and D. Regruto, "Combined automatic lane-keeping and driver's steering through a 2-DOF control strategy," *IEEE Transactions on Control Systems Technology*, vol. 17, no. 1, pp. 135–142, 2009.

[8] M. Aeberhard, S. Rauch, M. Bahram, G. Tanzmeister, J. Thomas, Y. Pilat, F. Homm, W. Huber, and N. Kaempchen, "Experience, results and lessons learned from automated driving on Germany's highways," *IEEE Intelligent Transportation Systems Magazine*, vol. 7, no. 1, pp. 42–57, 2015.

[9] A. Rupp and M. Stolz, "Survey on Control Schemes for Automated Driving on Highways," in *Automated Driving*. Springer, 2017, pp. 43–69.

[10] G. Tagne, R. Talj, and A. Charara, "Design and Comparison of Robust Nonlinear Controllers for the Lateral Dynamics of Intelligent Vehicles," *IEEE Transactions on Intelligent Transportation Systems*, vol. 17, no. 3, pp. 796–809, 2016.

[11] Z. Lu, B. Shyrokau, B. Boulkroune, S. V. Aalst, and R. Happee, "Performance Benchmark of state-of-the-art Lateral Path-following Controllers," in *2018 IEEE 15th International Workshop on Advanced Motion Control (AMC)*, 2018, pp. 541–546.

[12] T. Keviczky, P. Falcone, F. Borrelli, J. Asgari, and D. Hrovat, "Predictive control approach to autonomous vehicle steering," *2006 American Control Conference*, pp. 4670–4675, 2006.

[13] P. Falcone, H. Eric Tseng, F. Borrelli, J. Asgari, and D. Hrovat, "MPC-based yaw and lateral stabilisation via active front steering and braking," *Vehicle System Dynamics*, vol. 46, no. March 2015, pp. 611–628, 2008.

[14] H. Yu, J. Duan, S. Taheri, H. Cheng, and Z. Qi, "A model predictive control approach combined unscented Kalman filter vehicle state estimation in intelligent vehicle trajectory tracking," *Advances in Mechanical Engineering*, vol. 7, no. 5, pp. 1–14, 2015.

[15] Y. Cao, F. Yu, and Z. Luo, "Generalized Predictive Control Based on Vehicle Path Following Strategy by Using Active Steering System," in *International Symposium on Advanced Vehicle Control 2016*, 2016.

[16] R. C. Rafaila, G. Livint, and F. A. Rusu, "Multivariable Nonlinear Predictive Control of Autonomous Vehicle Dynamics," in *2016 IEEE International Conference on Development and Application Systems (DAS)*, 2016, pp. 97–102.

[17] P. Falcone, F. Borrelli, H. E. Tseng, J. Asgari, and D. Hrovat, "Linear time-varying model predictive control and its application to active steering systems: Stability analysis and experimental validation," in *International Journal of Robust and Nonlinear Control*, vol. 18, no. 8, 2008, pp. 862–875.

[18] P. Falcone, F. Borrelli, H. Tseng, J. Asgari, and D. Hrovat, "A hierarchical Model Predictive Control framework for autonomous ground vehicles," in *2008 American Control Conference*, 2008, pp. 3719–3724.

[19] J. E. Naranjo, C. González, R. García, and T. De Pedro, "Lane-change fuzzy control in autonomous vehicles for the overtaking maneuver," *IEEE Transactions on Intelligent Transportation Systems*, vol. 9, no. 3, pp. 438–450, 2008.

[20] T. Luettel, M. Himmelsbach, and H. J. Wuensche, "Autonomous ground vehicles—Concepts and a path to the future," *Proceedings of the IEEE Special Centennial Issue*, vol. 100, pp. 1831–1839, 2012.

[21] M. Bojarski, D. Del Testa, D. Dworakowski, B. Firner, B. Flepp, P. Goyal, L. D. Jackel, M. Monfort, U. Muller, J. Zhang, and Others, "End to end learning for self-driving cars," *arXiv preprint arXiv:1604.07316*, 2016.

[22] S. Du, H. Guo, and A. Simpson, "Self-driving car steering angle prediction based on image recognition," *Department of Computer Science, Stanford University, Tech. Rep. CS231-626*, 2017.

[23] U. Muller, J. Ben, E. Cosatto, B. Flepp, and Y. L. Cun, "Off-road obstacle avoidance through end-to-end learning," in *Advances in neural information processing systems*, 2006, pp. 739–746.

[24] G. Tao, *Adaptive Control Design and Analysis*. John Wiley & Sons, 2003.

[25] M. Di Bernardo, A. Di Gaeta, U. Montanaro, and S. Santini, "Synthesis and experimental validation of the novel LQ-NEMCSI adaptive strategy on an electronic throttle valve," *IEEE Transactions on Control Systems Technology*, vol. 18, no. 6, pp. 1325–1337, 2010.

[26] A. Buonomano, U. Montanaro, A. Palombo, and S. Santini, "Building temperature control using an enhanced MRAC approach," in *2015 European Control Conference (ECC)*. IEEE, 2015, pp. 3629–3634.

[27] U. Montanaro, A. di Gaeta, and V. Giglio, "An MRAC approach for tracking and ripple attenuation of the common rail pressure for GDI engines," *IFAC Proceedings Volumes*, vol. 44, no. 1, pp. 4173–4180, 2011.

[28] A. Buonomano, U. Montanaro, A. Palombo, and S. Santini, "Dynamic building energy performance analysis: A new adaptive control strategy for stringent thermohygrometric indoor air requirements," *Applied Energy*, vol. 163, pp. 361–386, 2016.

[29] U. Montanaro and J. M. Olm, "Integral MRAC with Minimal Controller Synthesis and bounded adaptive gains: The continuous-time case," *Journal of the Franklin Institute*, vol. 353, no. 18, pp. 5040–5067, 2016.

[30] A. Buonomano, U. Montanaro, A. Palombo, and S. Santini, "Temperature and humidity adaptive control in multi-enclosed thermal zones under unexpected external disturbances," *Energy and Buildings*, vol. 135, pp. 263–285, 2017.

[31] R. Byrne and C. Abdallah, "Design of a model reference adaptive controller for vehicle road following," *Mathematical and computer modelling*, vol. 22, no. 4, pp. 343–354, 1995.

[32] T. Fukao, S. Miyasaka, K. Mori, N. Adachi, and K. Osuka, "Active steering systems based on model reference adaptive nonlinear control," in *IEEE Intelligent Transportation Systems*, 2001, pp. 502–507.

[33] ——, "Active steering systems based on model reference adaptive nonlinear control," *Vehicle System Dynamics*, vol. 42, no. 5, pp. 301–318, 2004.

[34] Z. T. Dydek, A. M. Annaswamy, and E. Lavretsky, "Adaptive control and the NASA X-15-3 flight revisited," *IEEE Control Systems*, vol. 30, no. 3, pp. 32–48, 2010.

[35] D. Shevitz and B. Paden, "Lyapunov stability theory of nonsmooth systems," *IEEE Transactions on Automatic Control*, vol. 39, no. 9, pp. 1910–1914, 1994.

[36] N. Fischer, R. Kamalapurkar, and W. E. Dixon, "LaSalle-Yoshizawa corollaries for nonsmooth systems," *IEEE Transactions on Automatic Control*, vol. 58, no. 9, pp. 2333–2338, 2001.

[37] J. Corts, "Discontinuous dynamical systems-a tutorial on solutions, nonsmooth analysis, and stability," *IEEE Control Systems Magazine*, vol. 28, no. 3, pp. 36–73, 2008.

[38] A. Schmeitz, J. Zegers, J. Ploeg, and M. Alirezaei, "Towards a generic lateral control concept for cooperative automated driving theoretical and experimental evaluation," in *2017 5th IEEE International Conference on Models and Technologies for Intelligent Transportation Systems (MT-ITS)*, 2017, pp. 134–139.

[39] R. Rajamani, "Lateral vehicle dynamics," in *Vehicle Dynamics and Control*, 2012, ch. 2, pp. 15–46.

[40] J. Cortes, "Discontinuous dynamical systems," *IEEE Control systems magazine*, vol. 28, no. 3, pp. 36–73, 2008.

[41] F. H. Clarke, *Optimization and nonsmooth analysis*. Siam, 1990, vol. 5.

[42] H. K. Khalil and J. Grizzle, *Nonlinear systems*, 2nd ed. Prentice hall Upper Saddle River, NJ, 2002.

[43] X.-w. Mu, Z.-s. Ding, and G.-f. Cheng, "Uniformly ultimate boundedness for discontinuous systems with time-delay," *Applied Mathematics and Mechanics (English Edition)*, vol. 32, no. 9, pp. 1187–1196, 2011.
[44] R. Rajamani, *Vehicle Dynamics and Control*. Springer Science \& Business Media, 2006.

Shilp Dixit received his MSc. in Automotive Technology from Eindhoven University of Technology, Eindhoven, The Netherlands in 2015. He is currently working towards his Ph.D. degree at the Centre of Automotive Engineering at University of Surrey, Guildford, UK. His research interests are vehicle dynamics and control, trajectory planning and tracking for autonomous vehicles, and intelligent vehicles.

Umberto Montanaro received the "Laurea" degree (M.Sc.) in Computer Science Engineering (cum laude first class with Hons.) from the University of Naples Federico II, Naples, Italy in 2005. Umberto Montanaro received the Ph.D. in Control Engineering and the PhD in Mechanical Engineering from the University of Naples Federico II, in 2009 and 2016, respectively. From 2010 to 2013 he was Research Fellow at the Italian National Research Council (Istituto Motori) and he served as temporary Lecturer in Automation and Process Control at the University of Naples Federico II. Currently, he is a Lecturer in Control Systems for Automotive Engineering at the Department of Mechanical Engineering Sciences of the University of Surrey, Guildford, UK. His research interests range from control theory to control application and include: adaptive control, control of piecewise affine systems, mechatronics and automotive systems, and connected autonomous vehicles.

Mehrdad Dianati is a Professor of Autonomous and Connected Vehicles at Warwick Manufacturing Group (WMG), University of Warwick, as well as, a visiting professor at 5G Innovation Centre (5GIC), University of Surrey, where he was previously a Professor. He has been involved in a number of national and international projects as the project leader and work-package leader in recent years. Prior to his academic endeavour, he have worked in the industry for more than 9 years as senior software/hardware developer and Director of R&D. He frequently provide voluntary services to the research community in various editorial roles; for example, he has served as an associate editor for the IEEE Transactions on Vehicular Technology, IET Communications and Wiley's Journal of Wireless Communications and Mobile.

Alexandros Mouzakitis is the head of the Electrical, Electronics and Software Engineering Research Department at Jaguar Land Rover. Dr Mouzakitis has over 15 years of technological and managerial experience especially in the area of automotive embedded systems. In his current role is responsible for leading a multidisciplinary research and technology department dedicated to deliver a portfolio of advanced research projects in the areas of human-machine interface, digital transformation, self-learning vehicle, smart/connected systems and onboard/off board data platforms. In his previous position within JLR, Dr Mouzakitis served as the head of the Model-based Product Engineering department responsible for model-based development and automated testing standards and processes.

Saber Fallah is an Associate Professor at the University of Surrey. Currently, he is the Director of Connected and Autonomous Vehicles Lab (CAV-Lab) within the department of Mechanical Engineering Sciences. Since joining University of Surrey, he has contributed to securing research funding from EPSRC, Innovate UK, EU, KTP, and industry.

Dr. Fallah's work has contributed to the state-of-the-art research in the areas of connected autonomous vehicles and advanced driver assistance systems. So far, his research has produced four patents and more than 40 peer reviewed publications in high-quality journals and well-known conferences. He is also co-author of a textbook entitled Electric and Hybrid Vehicles: Technologies, modeling and control, (A mechatronics approach) which has been published by John Wiley publishing company in 2014. The book addresses the fundamentals of mechatronic design in hybrid and electric vehicles. Moreover, He is the co-editor of the book of conference proceedings resulted from the organisation of the TAROS 2017 conference published by Springer in 2017.